Supporting Information

A molecular imprinting-based selectively regulated laccase-like nanozyme strategy for onsite visual colorimetric/fluorescent assay toward microcystins in environmental waters

Fengjiao He[a], Linpin Luo[b], Si Li[a], Xin Liu[c,*], Heng Wang[a], Nannan Qiu[d,*], Wentao Zhang[b], Yongning Wu[d], Yizhong Shen[a,*]

[a] *School of Food & Biological Engineering, Anhui Province Institute of Agricultural Products Processing Technology, Hefei University of Technology, Hefei 230009, China*

[b] *College of Food Science and Engineering, Northwest A&F University, Yangling, 712100, China*

[c] *Hubei Key Laboratory for Processing and Transformation of Agricultural Products, College of Food Science and Engineering, Wuhan Polytechnic University, Wuhan, 430023, China*

[d] *NHC Key Laboratory of Food Safety Risk Assessment, Chinese Academy of Medical Science (2019RU014), China National Center for Food Safety Risk Assessment, Beijing, 100021, China*

*Corresponding authors: E-mail address: yzshen@hfut.edu.cn (Y. Shen)
qiunannan@cfsa.net.cn (N. Qiu)
liuxinhook@whpu.edu.cn (X. Liu)

Table of Contents

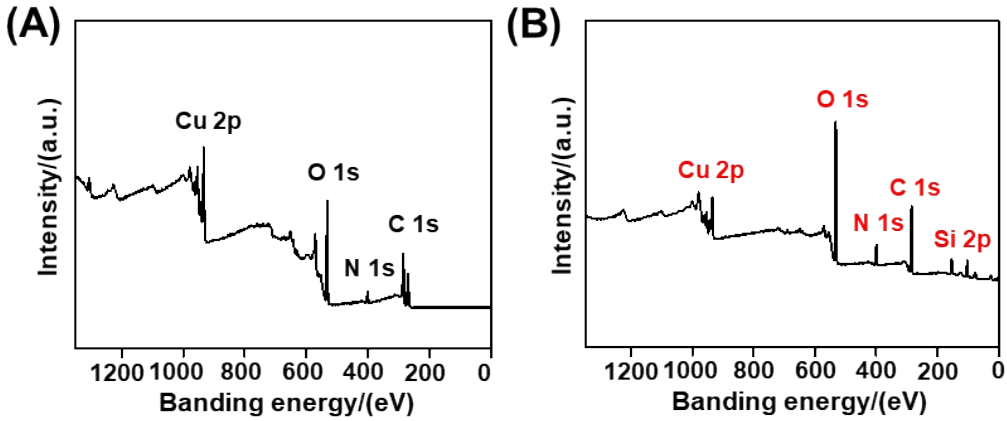

Fig. S1 XPS survey spectra of (A) Cu-CD and (B) MIP@Cu-CD.

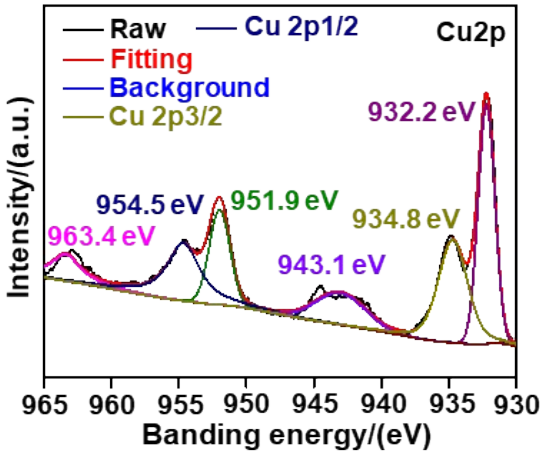

Fig. S2 XPS spectra of the Cu 2p region in the Cu-CD.

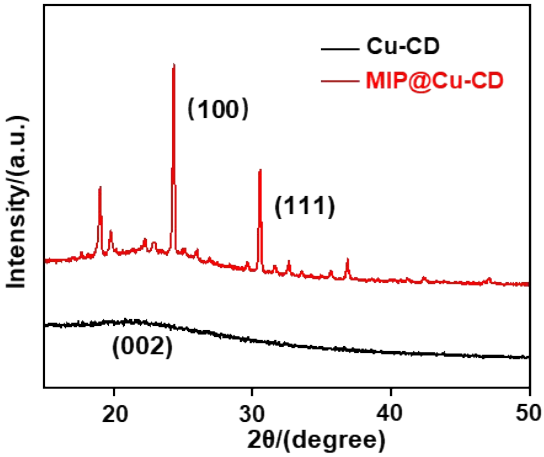

Fig. S3 XRD patterns of Cu-CD and MIP@Cu-CD.

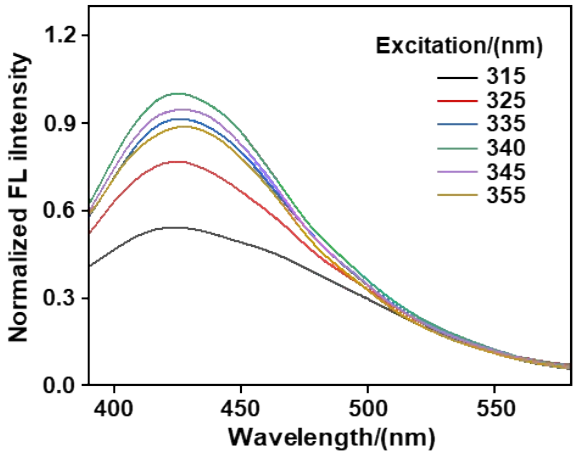

Fig. S4 Normalized fluorescence spectra of MIP@Cu-CD under different excitations. Experimental conditions: MIP@Cu-CD, 200.0 μg/mL; PBS buffer (pH = 7.5).

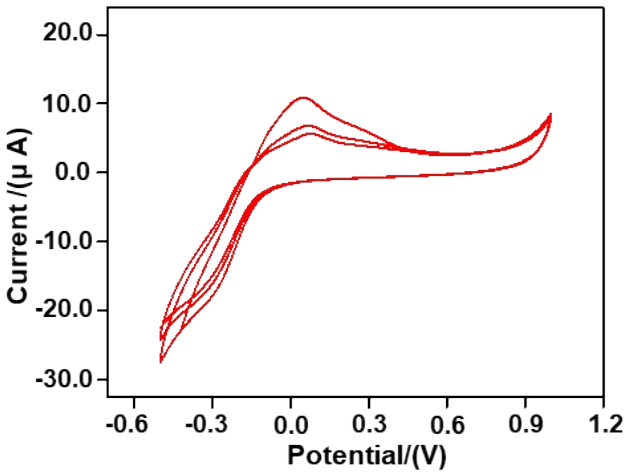

Fig. S5 Electrocatalytic performance testing of MIP@Cu-CD under different potentials. Experimental conditions: scan rate, 50.0 mV/s; reference electrode, Ag/AgCl; CV voltage range (V), -0.5~0.5 V; test atmosphere, nitrogen; effective area diameter of test electrode, 4.0 mm; electrolyte and concentration, 0.1 M NaAc buffer (pH = 5.0).

Table S1 Laccase-like catalytic activity of MIP@Cu-CD in comparison with other reported nanozymes.

Catalyst	K_m (mM)	V_{max} (10^{-7} M s^{-1})	*Ref.*
	2,4-DP	2,4-DP	
Laccase	0.41	1.068	1
CA-Cu	0.12	1.303	1
Cu-ZIF8	0.28	2.830	2
CeO_2@ZIF-8/Cu-CD	0.20	0.247	3
Cu_2Ov@Ce-TCPP	7.50	2.50	4
CN-MOF-818	4.481	0.628	5
EP-Cu	0.094	1.008	6
Cu/GMP	0.59	0.83	7
Cu_2O	0.20	1.083	8
MIP@Cu-CD	0.0228	2.075	This work

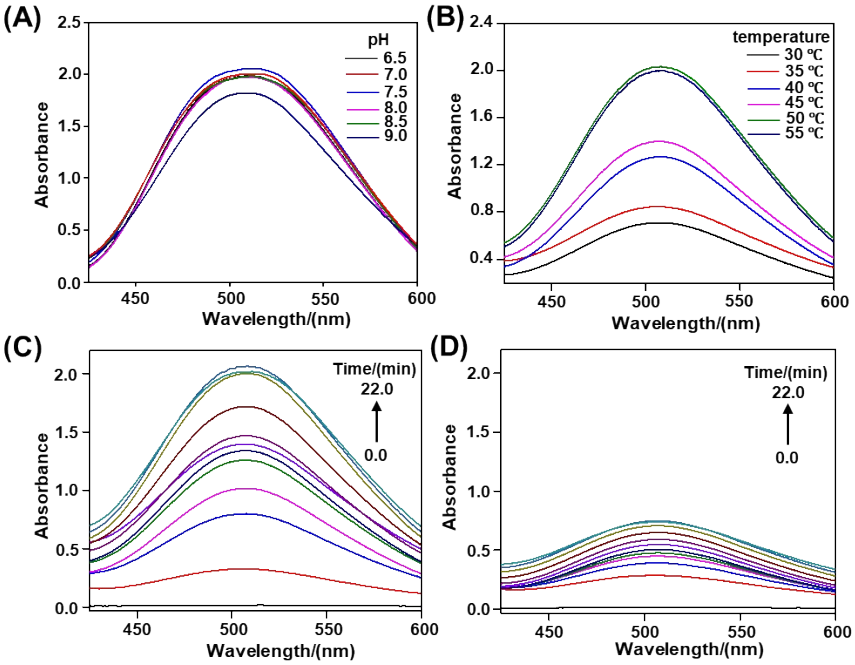

Fig. S6 Effect of reaction conditions on MIP@Cu-CD activity. Absorption spectra of MIP@Cu-CD + 2,4-DP + 4-AP at different (A) pH values, (B) temperature and (C) reaction time. (D) Absorption spectra of MIP@Cu-CD + MC-LR + 2,4-DP + 4-AP at different reaction time values. Experimental conditions: MIP@Cu-CD, 200.0 μg/mL; MC-LR, 800.0 μg/L; 2,4-DP, 1.0 mM; 4-AP, 1.0 mM; PBS buffer (pH = 7.5); 20.0 min; 50.0 ℃.

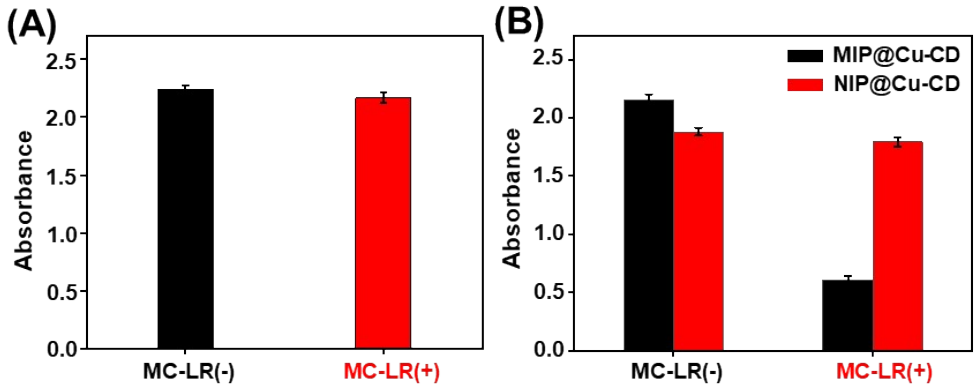

Fig. S7 (A) Absorbance at 510 nm of the Cu-CD + 2,4-DP + 4-AP system in the absence and presence of MC-LR. (B) Absorbance at 510 nm of MIP@Cu-CD + 2,4-DP + 4-AP and NIP@Cu-CD + 2,4-DP + 4-AP system in the absence and presence of MC-LR. Experimental conditions: Cu-CD, 200.0 μg/mL; MIP@Cu-CD, 200.0 μg/mL; NIP@Cu-CD, 200.0 μg/mL; MC-LR, 800.0 μg/L; 2,4-DP, 1.0 mM; 4-AP, 1.0 mM; PBS buffer (pH = 7.5); 20.0 min; 50.0 ℃.

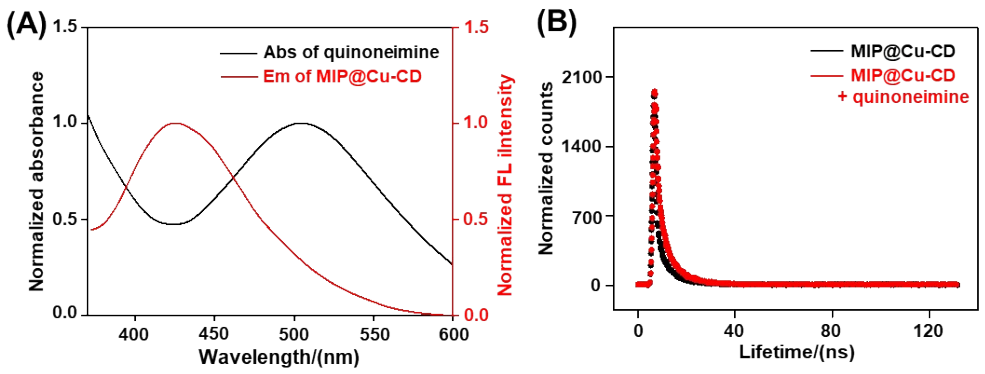

Fig. S8 (A) Normalized absorption spectra of quinoneimine (quinoneimine was determined by completely oxidizing trace amounts of 2,4-DP in the presence of 4-AP), and normalized emission spectra of MIP@Cu-CD in PBS buffer (pH = 7.5). (B) Fluorescence lifetime decay curves of MIP@Cu-CD before and after incubation with quinoneimine in PBS buffer (pH = 7.5). Experimental conditions: MIP@Cu-CD, 200.0 μg/mL; 2,4-DP, 1.0 mM; 4-AP, 1.0 mM; PBS buffer (pH = 7.5); 20.0 min; 50.0 ℃.

Table S2 Effect of different concentrations of quinoneimine (quinoneimine was determined by completely oxidizing trace amounts of 2,4-DP in the presence of 4-AP) on the decrease of the fluorescence intensity of MIP@Cu-CD at 420 nm in PBS buffer (pH = 7.5).

quinoneimine (μM)	A_{ex}	A_{em}	**CF**	F_{obs}	F_{corr}	E_{obs}	E_{corr}
0.0	0.323	0.176	1.697	61.53	104.43	0.000	0.000
5.0	0.411	0.222	1.942	52.9	102.74	0.140	0.016
10.0	0.471	0.263	2.146	47.53	102.02	0.228	0.023
15.0	0.522	0.288	2.311	42.84	98.98	0.304	0.052
20.0	0.562	0.336	2.519	38.72	97.54	0.371	0.066
25.0	0.602	0.35	2.650	36.57	96.90	0.406	0.072

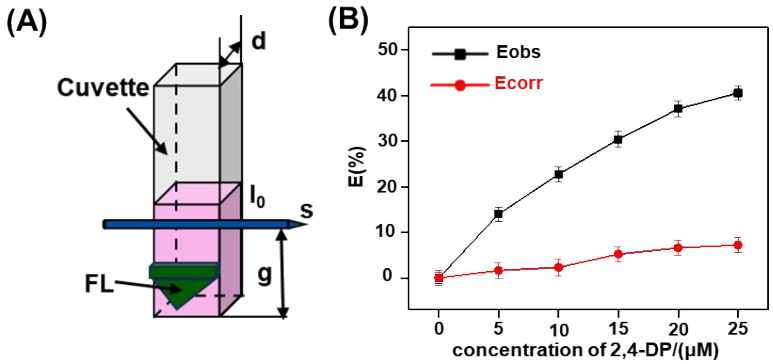

Fig. S9 (A) This part illustrates how varying concentrations of 2,4-DP impact the reduction of IFE fluorescence from MIP@Cu-CD at 420 nm. The distance between the excitation beam and the cuvette's edge is g = 0.4 cm, with the cuvette's outer diameter being d = 1.0 cm and its inner diameter s = 0.10 cm. I_0 denotes the excitation light, while FL represents the resulting fluorescence. (B) Observed and corrected values of fluorescence quenching of MIP@Cu-CD induced by 2,4-DP. The efficiency is determined using the equation: $E = (F_0 - F)/F_0$. In this equation, F denotes the fluorescence intensity of MIP@Cu-CD at 420 nm after it has interacted with various concentrations of 2,4-DP. Conversely, F_0 refers to the fluorescence intensity of MIP@Cu-CD at 420 nm when 2,4-DP is not present.

The calibrated fluorescence emission intensity is determined by the equation provided below:

$$CF = \frac{F_{\text{corr}}}{F_{obs}} = \frac{2.3dA_{ex}}{1-10^{-dA_{ex}}} \times 10^{gA_{em}} \times \frac{2.3sA_{em}}{1-10^{-sA_{em}}} \qquad \text{Eq. 1}$$

In Eq. 1, CF represents the correction factor. F_{obs} is the fluorescence intensity measured at 420 nm, while F_{corr} is the corrected fluorescence intensity at 420 nm, accounting for the absence of the IFE effect. Additionally, A_{em} and A_{ex} refer to the emission wavelength and the absorbance per centimeter, respectively. The notable difference between E_{obs} and E_{corr} indicates that the fluorescence quenching is a result of IFE behavior.

Note S1: There was a spectral overlapping between the absorption of quinoneimine and the fluorescence emission of MIP@Cu-CD, suggesting that the blue fluorescence quenching at 420 nm may be due to either fluorescence resonance energy transfer (FRET) from the produced quinoneimine to the MIP@Cu-CD or the inner filter effect (IFE).[9] The negligible change in the fluorescence lifetime of MIP@Cu-CD before (~5.45 ns) and after (~5.61 ns) incubation with quinoneimine rules out the FRET

involvement.[10] Furthermore, the observed fluorescence quenching efficiency (E_{obs}) was considerably higher than the corrected bursting efficiency (E_{corr}, after accounting for the IFE), confirming the significant role of the IFE on the blue fluorescence quenching of MIP@Cu-CD at 420 nm.[11]

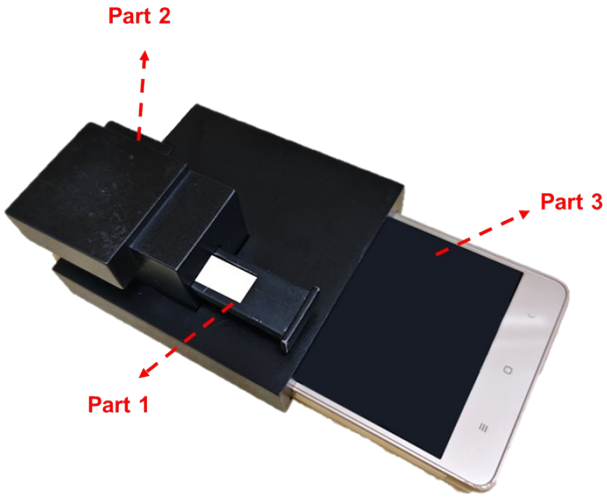

Fig. S10 Diagram of the home-made smartphone-auxiliary portable device. Part 1: a sample chamber for filter paper strips. Part 2: a built-in 365 nm LED ultraviolet light-emitting diode (3.0 W). Part 3: a smartphone for image acquisition and RGB value analysis.

Table S3 Comparison of the analytical parameters of the MIP@Cu-CD + 2,4-DP + 4-AP for MC-LR detection with other reported methods.

Methods	**Materials**	**Linear range (μg/L)**	**Detection limit (μg/L)**	***Ref.***
Fluorescence	QDs	0.25 − 5.0	0.1	12
HPLC-UV	–	–	0.3	13
OS-ELISA	–	1.4×10^{-1} – 1.0×10^{4}	0.14	14
Immunosensor	$ZnFe_2O_4$ MNPs	0.6 − 5.0	0.10	15
Optical biosensor	PAA-IPN	3.8 − 150.0	0.88	16
Fluorescence	SWNTs	3.98×10^{-1} – 1.19×10^{3}	0.14	17
LFA	AuNPs	1.0 – 50.0	2.5	18
ECL	SQD	1.0×10^{-3} – 1.0×10^{2}	0.17	19
Colorimetric & Fluorescence	MIP@Cu-CD	0.76 – 800.0 0.34 – 800.0	0.227 0.101	This work

References

1. X. Xu, J. Wang, R. Huang, W. Qi, R. Su and Z. He, Preparation of laccase mimicking nanozymes and their catalytic oxidation of phenolic pollutants, *Catal. Sci. Technol*., 2021, **11**, 3402-3410.

2. S. K. Safavi–Mirmahaleh and Z. Moradi-Shoeili, Laccase-like nanozyme fabricated by Cu^{2+}-doped ZIF8 for dopamine determination and catalytic degradation of phenolic pollutants, *Colloid. Polym. Sci.*, 2025, **303**, 185-196.

3. Q. Yin, Y. Wang, D. Yang, Y. Yang and Y. Zhu, A colorimetric detection of dopamine in urine and serum based on the CeO_2@ZIF-8/Cu-CDs laccase-like nanozyme activity, *Luminescence*, 2024, **39**, e4684.

4. F. Xiao, Q. Xia, S. Zhang, Q. Li, D. Chen, H. Li, D. Yang and Y. Yang, Ultrasound and defect engineering-enhanced nanozyme with high laccase-like activity for oxidation and detection of phenolic compounds and adrenaline, *J. Hazard. Mater*., 2024, **465**, 133126.

5. X. Liu, P. An, Y. Han, H. Meng and X. Zhang, MOF-818(Cu)-derived bi-nanozymes of laccase and catecholase mimics and colorimetric sensing to epinephrine, *Microchem. J*., 2024, **201**, 110559.

6. Q. Wang, Y. Hou, M. Lin and Q. Yang, Construction of extracellular peptide laccase-mimic nanozyme for the detection and degradation of phenols pollutants, *Colloids Surf. A Physicochem. Eng. Aspects*., 2024, **699**, 134687.

7. H. Liang, F. Lin, Z. Zhang, B. Liu, S. Jiang, Q. Yuan and J. Liu, Multicopper laccase mimicking nanozymes with nucleotides as ligands, *ACS Appl. Mater. Interfaces*., 2017, **9**, 1352-136.

8. T. Maity, S. Jain, M. Solra, S. Barman and S. Rana, Robust and reusable laccase mimetic copper oxide nanozyme for phenolic oxidation and biosensing, *ACS Sustain. Chem. Eng*., 2022, **10**, 1398-1407.

9. G. Wu, S. Liu, C. Du, M. Huang, Y. Wu and Y. Shen, A versatile visual molecular imprinting-driven switchable nanozyme activity-based trimodal assay and logic gate circuits of ethyl carbamate, *Anal. Chem*., 2024, **96**, 14706-14713.

10. C. Guo, J. Zhai, Y. Wang, W. Yang and X. Xie, Wash-free detection of nucleic acids with photoswitch-mediated fluorescence resonance energy transfer against optical background interference, *Anal. Chem*., 2021, **93**, 8128-8133.

11. E. Sheng, Y. Lu, Y. Tan, Y. Xiao, Z. Li and Z. Dai, Ratiometric fluorescent quantum dot-based biosensor for chlorothalonil detection via an inner-filter effect, *Anal. Chem*., 2020, **92,** 4364-4370.

12. J. Sun, Y. Li, F. Pi, J. Ji, Y. Zhang and X. Sun, Using fluorescence immunochromatographic test strips based on quantum dots for the rapid and sensitive determination of microcystin-LR, *Anal. Bioanal. Chem*., 2017, **409**, 2213-2220.

13. A. Padovan, K. Kennedy and K. Gibb, A microcystin synthesis *mcyE/ndaF* gene assay enables early detection of microcystin production in a tropical wastewater pond, *Harmful Algae*, 2023, **127**, 102476.

14. L. Chen, R. Tan, Y. Zhou, L. Zhang, S. Zhang, X. Li, Y. Cong, H. Li, P. Sun, H. Ueda and J. Dong, Development of an open sandwich ELISA for the detection of microcystin-LR, *Microchem. J*., 2020, **158**, 105325.

15. L. Zhao, L. Teng, J. Zhang and H. Li, Point-of-care detection of microcystin-LR with a personal glucose meter in drinking water source, *Chin. Chem. Let*., 2019, **30**, 1035-1037.

16. S. Hussain, A. Al-Tabban and M. Zourob, Aptameric photonic structure-based optical biosensor for the detection of microcystin, *Biosens. Bioelectron*., 2024, **260**, 116413.

17. S. M. Taghdisi, N. M. Danesh, M. Ramezani, N. Ghows, S. A. Mousavi Shaegh and K. Abnous, A novel fluorescent aptasensor for ultrasensitive detection of microcystin-LR based on single-walled carbon nanotubes and dapoxyl, *Talanta*, 2017, **166**, 187-192.

18. J. Feng, Y. Wu, J. Zhang, R. Jin, Y. Li and Q. Shen, An aptamer lateral flow assay for visual detection of microcystins-LR residue in fish, *J. Food Compos. Anal*., 2023, **115**, 105012.

19. Y. Han, Y. Du, K. Xu, X. Ren, G. Zhao, Z. Ru, Y. Jia and Q. Wei, Sulfur quantum dot-based electrochemiluminescence resonance energy transfer system for a dual-mode ultrasensitive detection of MC-LR using Ag^{+} as a signal amplification switch, Anal. Chem., 2023, **95**, 8679-8686.